Journal Pre-proofs

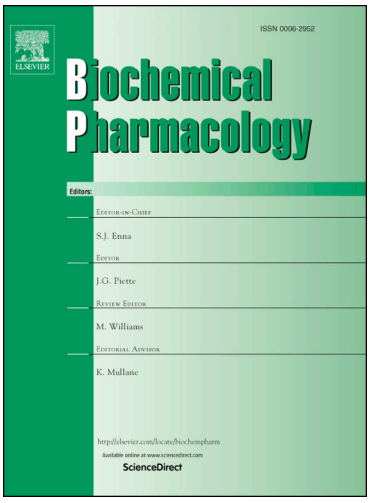

Characterisation of tyrosine kinase inhibitor-receptor interactions at VEGFR2 using sunitinib-red and nanoBRET

Marieke Van Daele, Laura E Kilpatrick, Jeanette Woolard, Stephen J Hill

PII: S0006-2952(23)00263-0
DOI: https://doi.org/10.1016/j.bcp.2023.115672
Reference: BCP 115672

To appear in: *Biochemical Pharmacology*

Received Date: 24 April 2023
Revised Date: 13 June 2023
Accepted Date: 26 June 2023

Please cite this article as: M. Van Daele, L.E. Kilpatrick, J. Woolard, S.J. Hill, Characterisation of tyrosine kinase inhibitor-receptor interactions at VEGFR2 using sunitinib-red and nanoBRET, *Biochemical Pharmacology* (2023), doi: https://doi.org/10.1016/j.bcp.2023.115672

Characterisation of tyrosine kinase inhibitor-receptor interactions at VEGFR2 using sunitinib-red and nanoBRET.

Marieke Van Daele[1,2], Laura E Kilpatrick[2,3], Jeanette Woolard[1,2], Stephen J Hill[1,2,*],

[1] Division of Physiology, Pharmacology and Neuroscience, School of Life Sciences, University of Nottingham, Nottingham NG7 2UH, UK

[2] Centre of Membrane Proteins and Receptors, University of Birmingham and Nottingham, The Midlands, UK

[3] Division of Bimolecular Science and Medicinal Chemistry, School of Pharmacy, Biodiscovery Institute, University of Nottingham, NG7 2RD, UK

*Corresponding authors and persons to whom material requests should be addressed:

Stephen J. Hill, Division of Physiology, Pharmacology and Neuroscience, School of Life Sciences, University of Nottingham, Nottingham, NG7 2UH, UK: stephen.hill@nottingham.ac.uk

Jeanette Woolard, Division of Physiology, Pharmacology and Neuroscience, School of Life Sciences, University of Nottingham, Nottingham, NG7 2UH, UK: jeanette.woolard@Nottingham.ac.uk

Abstract (246/250 words)

Vascular endothelial growth factor (VEGF) is an important mediator of angiogenesis, proliferation and migration of vascular endothelial cells. It is well known that cardiovascular safety liability for a wide range of small molecule tyrosine kinase inhibitors (TKIs) can result from interference with the VEGFR2 signalling system. In this study we have developed a ligand-binding assay using a fluorescent analogue of sunitinib (sunitinib-red) and full length VEGFR2 tagged on its C-terminus with the bioluminescent protein nanoluciferase to monitor ligand-binding to VEGFR2 using bioluminescence resonance energy transfer (BRET). This NanoBRET assay is a proximity-based assay (requiring the fluorescent and bioluminescent components to be within 10nm of each other) that can monitor the binding of ligands to the kinase domain of VEGFR2. Sunitinib-red was not membrane permeable but was able to monitor the binding affinity and kinetics of a range of TKIs in cell lysates. Kinetic studies showed that sunitinib-red bound rapidly to VEGFR2 at 25 °C and that cediranib had slower binding kinetics with an average residence time of 112 min. Comparison between the log K_i values for inhibition of binding of sunitinib-red and log IC_{50} values for attenuation of $VEGF_{165}$a-stimulated NFAT responses showed very similar values for compounds that inhibited sunitinib-red binding. However, two compounds that failed to inhibit sunitinib-red binding (dasatinib and entospletinib) were still able to attenuate VEGFR2-mediated NFAT signalling through inhibition of downstream signalling events. These results suggest that these compounds may still exhibit cardiovascular liabilities as a result of interference with downstream VEGFR2 signalling.

Key words:

VEGFR2, NanoBRET, sunitinib-red, tyrosine kinase inhibitors, NFAT, ligand-binding

Abbreviations:

BRET, Bioluminescence resonance energy transfer; BSA, Bovine serum albumin; DMEM, Dulbecco's Modified Eagle's Medium; FCS, Fetal calf serum; HBSS, HEPES buffered salt solution; IP3, Inositol 1,4,5-trisphosphate; ITAMs, Immunoreceptor tyrosine-based activation motifs; NFAT, Nuclear factor of activated T-cells; NFAT-RE, NFAT response element; NLuc-VEGFR2, N-terminal nanoluciferase-tagged VEGFR2; PBS, Phosphate buffered saline; PIP2, Phosphinositide 4,4-bisphosphate; PLCγ, Phospholipase Cγ; RTKs, Receptor tyrosine kinases; SEM, Standard error of mean; SH2, SRC homology 2; SYK, Spleen associated tyrosine kinase; TKIs, Tyrosine kinase inhibitors; VEGF, Vascular endothelial growth factor; VEGFR2-NLuc, C-terminal nanoluciferase-tagged VEGFR2.

1. Introduction

Vascular Endothelial Growth Factor (VEGF) is an antiparallel dimeric protein that acts as a key signalling molecule in angiogenesis [1-5]. Ligands of the VEGF family act by binding to one of three cell surface receptor tyrosine kinases (RTKs), namely VEGFR1, VEGFR2 and VEGFR3 or the VEGFR coreceptor neuropilin-1 [5]. Binding of $VEGF_{165}$a, the most abundant VEGF-A isoform, to VEGFR2 is a hallmark of vascular development and angiogenesis since it promotes the proliferation, survival, and migration of vascular endothelial cells [1, 5, 6,7]. Additionally, VEGFR2 signalling plays a pivotal role in pathological conditions, including diabetic retinopathy and cancer [1,7]. Whereas angiogenesis is a well-regulated process in normal physiological circumstances, this balance is disrupted in cancer. Pro-angiogenic factors, secreted by tumour cells, dominate, and create a pro-vascularization micro-environment [8–10]. Growth of a tumour beyond the size of 1 – 2 mm^3 is dependent on angiogenesis to meet the high demand of cancer cells for nutrients and oxygen [1, 7, 11]. Most human tumours overexpress VEGF mRNA and many *in vitro* tumour cell lines upregulate its receptors, emphasizing its crucial role as a mediator in tumour angiogenesis [1,7,12].

To inhibit angiogenesis in cancer, therapeutic agents interfering with the VEGF signalling pathway have been developed including VEGF-A targeted antibodies and small molecule tyrosine kinase inhibitors (TKIs) 1,7,13]. The hydrophobic small molecule inhibitors pass through the cell membrane, where they target the intracellular ATP-binding site of the VEGFR2 kinase domain and inhibit its downstream signalling pathways [8,13]. Sunitinib (Sutent®) for example, was approved in 2007 for advanced renal cell carcinoma [12,14], and later also marketed for treatment of gastrointestinal stromal tumours [14] and pancreatic cancer [12].

With both VEGF-A targeting antibodies and TKIs, hypertension and proteinuria are frequently reported side effects [12,15,16]. Generally, drugs inhibiting VEGFR2 with a higher relative potency compared to other tyrosine kinases, result in higher rates of elevated blood pressure than less potent VEGFR2 inhibitors [15, 17,18]. Other multi-kinase inhibitors display a similar cardiovascular safety profile which may be a consequence of their off-target effects on VEGFR2. For example, fostamatinib and its active metabolite R406 were designed to bind to a cytoplasmic tyrosine kinase, spleen associated tyrosine kinase (SYK) [19,20]. However, this compound has been identified as a VEGFR2 inhibitor [21] and its clinical use in chronic immune thrombocytopenia is associated with raised blood pressure [19,20,22]. To improve the safety liabilities observed with fostamatinib, a second generation of SYK inhibitors, including entospletinib, with a better selectivity profile was developed, to achieve higher levels of SYK inhibition without the onset of dose-limiting adverse drug reactions [23, 24].

SYK is a particularly interesting tyrosine kinase since it appears to have a crucial role in adaptive immune signalling as well as a range of other diverse biological functions including cellular adhesion, platelet activation and vascular development [25]. SYK contains two tandem SRC homology 2 (SH2) domains that can interact with dual-phosphorylated immunoreceptor tyrosine-based activation motifs (ITAMs) on their target proteins (e.g. the intracellular tail of the Fc receptor IIA; [25]). Some target proteins for SYK contain only one ITAM sequence (Hemi-ITAM) but can generate the SYK binding site following dimerization (e.g. CLEC2; [25,26,27]). Interestingly, VEGFR2 has a hemi-ITAM sequence beginning at Y1175 and VEGFR2 may be able to activate SYK following ligand-induced VEGFR2 receptor dimerization [28]. Phosphorylation of Y1175 recruits PLCγ, triggering Ca^{2+}-dependent signalling, and is involved in endothelial cell migration [5]. SYK inhibitors have been shown to reduce phosphorylation of Y1175 but not that of other tyrosine residues in VEGFR2 (e.g. Y1054 in the activation loop; [5,29]). It is therefore possible that SYK inhibitors may reduce

VEGFR2-signalling independently of a direct inhibition of the intrinsic kinase activity of VEGFR2.

The hypertension induced by fostamatinib demonstrates the importance of identifying at an early stage the cardiovascular safety liabilities resulting from interference with the VEGFR2 signalling system for a wide range of TKIs where dose-limiting hypertension may be an important side effect [29]. Previously Carter *et al*. (2015; [30]) described a downstream nuclear factor of activated T-cells (NFAT)-luciferase assay to monitor the pharmacological interaction of TKIs with the $VEGF_{165}$a/VEGFR2 signalling system. Here we have used a fluorescent analogue of sunitinib and bioluminescence resonance energy transfer (BRET) to directly monitor the binding of TKIs to VEGFR2. This is based on a proximity-based assay (requiring the fluorescent and bioluminescent components to be within 10nm of each other) that can quantify interactions between fluorescent sunitinib and the C-terminus of VEGFR2 tagged with the bioluminescent protein nanoluciferase [31-33]. The effect of a range of TKIs on VEGFR2 ligand binding and signalling have then been compared and we report that the second generation SYK inhibitor entospletinib and the BCR-ABL inhibitor dasatinib can inhibit VEGFR2 NFAT signalling in HEK293 cells without inhibiting the direct binding of sunitinib-red to VEGFR2.

2. Materials and methods

2.1 Materials, cell lines and VEGFR2-NLuc construct

Recombinant human $VEGF_{165}a$ was purchased from R&D Systems (Abingdon, UK). Sunitinib-red was purchased from PerkinElmer Ltd (Beaconsfield, UK). Sunitinib, cediranib, erlotinib, dasatinib, motesanib, fostamatinib, R406, cerdulatinib and entospletinib were purchased from ApexBio (Houston, USA). FuGENE HD Transfection Reagent, One-Glo® luciferase, furimazine and NanoGlo® HiBiT lytic buffer were obtained from Promega Corporation (Madison, USA). The NFAT-ReLuc2P NLuc-VEGFR2 HEK293 cell line has been described previously (Kilpatrick et al., 2017). HEK293T cells were obtained from ATCC (Manassas, USA). The NFAT-ReLuc2P HEK293 cell line was obtained from Promega Corporation (Madison, USA). The VEGFR2-NLuc cDNA construct was a generous gift from Promega Corporation (Madison, USA). Both cell lines were used between passage 10 and 30. No further authentication of cell lines was performed and HEK293 cell lines are not listed in the ICLAL register of commonly misidentified cell lines; www.iclac.org).

2.2 Cell culture

All HEK293 cell lines were cultured in Dulbecco's Modified Eagle's Medium (DMEM, Sigma-Aldrich, Gillingham, UK), supplemented with 10% fetal calf serum (FCS, Sigma Aldrich, Gillingham, UK) at 37 °C/5% CO_2. Cells passaging was performed at 80 – 90% confluency using phosphate buffered saline (PBS, Sigma Aldrich, Gillingham, UK) and trypsin (0.25% w/v in versene, Gillingham, UK). Transient transfection was performed using FuGENE HD, according to the manufacturer's instructions, at a cDNA to reagent ratio of 1:3 in OptiMEM (Thermo-Fisher Scientific, Waltham, USA).

2.3 Measuring sunitinib-red binding using NanoBRET.

HEK293T cells were grown to 80% confluency in DMEM/10% FCS. Cells were normally seeded 48h prior to assay at 20,000 cells/well in DMEM/10% FCS in white 96 well plates (Greiner Bio-One, Stonehouse, UK), coated with 0.01 $mg.mL^{-1}$ poly-D-lysine (Sigma Aldrich, Gillingham, UK) in PBS. The next day, cells were transfected with the VEGFR2-NLuc construct (0.1 μg cDNA/well) and incubated for a further 24 h. On the day of the experiment, medium was removed and replaced with HEPES Buffered Salt Solution (HBSS; 10 mM HEPES (Sigma Aldrich, Gillingham, UK), 10 mM glucose (Thermo-Fisher Scientific, Waltham, USA), 146 mM NaCl (VWR Chemicals, Lutterworth, UK), 5 mM KCl (VWR Chemicals, Lutterworth, UK), 1 mM $MgSO_4$ (Sigma Aldrich, Gillingham, UK), 2 mM sodium pyruvate (Sigma Aldrich, Gillingham, UK), 1.3 mM $CaCl_2$ (Sigma Aldrich, Gillingham, UK); pH 7.2)/0.1% protease-free bovine serum albumin (BSA, Sigma Aldrich, Gillingham, UK). Cells were pre-treated with 1 nM $VEGF_{165}a$ for 15 min, followed by fluorescent ligand and inhibitor where appropriate, in a total volume of 50 μL per well, and incubated for 1 h at 37 °C/5% CO_2. Furimazine (1:400) was added to each well and plates were incubated for a further 10 minutes at 25 °C/5% CO_2 before BRET was measured. Cells were then lysed using NanoGlo® lytic buffer at 25 °C for 10 minutes before BRET was measured a second time. Fluorescence and bioluminescence were read at 25 °C using a PHERAstar FS plate reader (BMG Labtech, Ortenberg, Germany) using 460nm (80nm bandpass) (donor NanoLuc emission) and > 610nm longpass (acceptor sunitinib-red emission) filters. A gain of 3600 was used for the 610nm channel and a gain of 1400 for the 460nm channel. Raw BRET ratios were calculated from the ratio of acceptor to donor emission values.

For ligand-binding saturation assays with increasing concentrations (0 to 1000nM) of sunitinib-red, assays were undertaken in white half-well 96 well plates (Corning Incorporated, New

York, USA) in order to conserve fluorescent reagent. In these experiments, a total volume of 25 μl was used, and each well was plated with 10,000 cells and transfected with 0.05 ug cDNA. 100 μM cediranib was used to define non-specific binding. A gain of 3600 was used for the 610nm PHERAstar FS channel and a gain of 2400 for the 460nm channel.

2.4 NanoBRET kinetic assays.

For kinetic measurements of sunitinib-red binding, HEK293T cells were seeded and transfected as described above. Cells were then pre-treated with 1 nM $VEGF_{165}a$ for 15 minutes, followed by addition of sunitinib-red and the appropriate inhibitor in triplicates. Plates were incubated at 37 °C/5% CO_2 for 1 h before furimazine (1:400) was added. Baseline BRET was taken for 10 minutes every 60s. Cell lysis was then performed, and BRET was measured every 60 seconds for a further 50 minutes at either 25 °C or 37 °C. In some experiments, following the treatment of cells with 1nM $VEGF_{165}a$ for 15 mins, furimazine (1:400) and NanoGlo® lytic buffer were added simultaneously and baseline BRET measurement commenced immediately every 60s at 25 °C or 37 °C. After 10 minutes, sunitinib-red and the appropriate inhibitor were added in triplicates, and BRET was measured every 60 seconds for a further 50 minutes.

2.5 NFAT luciferase reporter gene assay.

HEK293T cells stably expressing both NLuc-VEGFR2 and the Firefly luciferase reporter gene ReLuc2P (Promega Corporation, USA) inserted downstream of the NFAT promoter were used to monitor NFAT-induced gene transcription following VEGFR2 activation [33]. Cells were grown to 80% confluency in DMEM/10% FCS. Cells were seeded 48h prior to experimentation at 20,000 cells/well in DMEM/10% FCS in white 96 well plates, coated with 0.1 $mg.mL^{-1}$ poly-D-lysine in PBS. After 24 h, medium was replaced by 100 μL serum-free DMEM and cells were incubated for a further 24 h. On the day of the experiment, medium was replaced by serum-free DMEM/0.1% BSA. In the appropriate wells, cells were pre-treated with increasing concentrations of inhibitor in triplicate for 1 h. $VEGF_{165}a$ or ionomycin calcium salt (Sigma Aldrich, Gillingham, UK) was then added to the wells in a total volume of 100 μL/well and plates were incubated for 5 h. Consequently, medium was replaced by 50 μL/well serum-free DMEM/0.1% BSA and 50 μL/well ONE-Glo luciferase reagent. Following a 5-minute delay, luminescence was measured by a TopCount plate reader (Perkin Elmer, Buckingham, UK).

2.6 Data analysis and statistical tests.

All data were analysed using Prism 9.4.1 (GraphPad Software, San Diego, CA, USA) and are presented as mean ± SEM. The sunitinib-red saturation curve was fitted simultaneously for total and non-specific binding using a one site fit, to the following equation:

$$Total\ binding = B_{max} \cdot \frac{[L]}{[L] + K_D} + M.[L] + C$$

where B_{max} is the maximal specific binding, [L] is the concentration of sunitinib-red (nM), K_D is the equilibrium dissociation constant of sunitinib-red (nM), M is the slope of the non-specific binding component and C the y-axis intercepts.

The $VEGF_{165}a$ concentration-response data were normalized to responses to 10 nM $VEGF_{165}a$ and fitted to a non-linear regression with the following equation:

$$Response = \frac{E_{max} \text{ x } [A]^{Hc}}{[A]^{Hc} + EC_{50}^{Hc}}$$

where E_{max} is the maximal response, [A] is the concentration of $VEGF_{165}a$, EC_{50} is the concentration of $VEGF_{165}a$ required to generate 50% of the E_{max} and Hc is the Hill coefficient, representing the slope of the curve.

Displacement and inhibition curves of unlabelled inhibitors, in the presence of a fixed concentration of sunitinib-red in the nanoBRET assay or $VEGF_{165}a$ in the NFAT assay, were fitted to the following equation:

$$Specific\ binding\ or\ Response = 100 - \frac{100 \text{ x } [I]^{Hc}}{[I]^{Hc} + IC_{50}^{Hc}}$$

where specific binding is the specific binding of 30 nM sunitinib-red, response is the response to 1nM $VEGF_{165}a$ alone, [I] is the concentration of inhibitor, IC_{50} is the concentration of inhibitor required to generate 50% of inhibition, and Hc is the Hill coefficient, describing the steepness of the curve.

Binding affinities (K_i) of unlabelled inhibitors were calculated using the Cheng-Prusoff equation:

$$K_i = \frac{IC_{50}}{1 + \frac{[L]}{K_D}}$$

Where IC_{50} is the inhibitor concentration required to generate 50% of inhibition, [L] is the concentration of sunitinib-red used (30nM), and K_D was derived from the sunitinib-red saturation binding curve.

The biphasic inhibition curve for inhibition of sunitinib-red binding by non-fluorescent sunitinib was fitted to the following equation:

$$Specific\ binding = (100 - \frac{100\ \text{x}\ [Sun]}{[Sun] + IC_{50}}) + \frac{E_{MAX}\ \text{x}\ [Sun]}{[Sun] + EC_{50}}$$

where specific binding is the specific binding of 30 nM sunitinib-red alone, [Sun] is the concentration of non-fluorescent sunitinib, IC_{50} is the concentration of sunitinib required to inhibit 50% of the specific binding of 30 nM sunitinib-red and E_{MAX} and EC_{50} are the maximal BRET signal and concentration of sunitinib required to stimulate a direct BRET response.

For NanoBRET association kinetic studies, the BRET ratio obtained immediately before addition of sunitinib-red was subtracted from the subsequent BRET ratios obtained at each time point for each concentration (L) of fluorescent sunitinib-red. The data were then simultaneously fit to the following equations:

$$Y = Y_{max}\,(1 - e^{-k_{obs}.t}).$$

$$k_{on} = \frac{k_{obs} - k_{off}}{[L]}$$

where Y_{max} equals the level of binding at infinite time (t), k_{obs} is the rate constant for the observed rate of association at a particular concentration of L, [L] is the ligand concentration in molar, k_{off} is the dissociation rate constant of the ligand in per minute and k_{on} is the association rate constant in per molar per minute. From this, the kinetic dissociation constant (K_D) is determined as follows:

$$K_D = \frac{k_{off}}{k_{on}}$$

The binding kinetics of unlabelled ligands was quantified using the competition association assay based on the theoretical framework by Motulsky and Mahan (1984; [34]). NanoBRET data were fitted to this framework in GraphPad Prism using the competition association model to determine association and dissociation rate constants of the unlabelled TKIs.

Statistical significance was determined by Student's paired t-test, unpaired t test or one-way ANOVA and where $p < 0.05$ was considered statistically significant throughout this study.

3. Results.

3.1 Binding of sunitinib-red to C-terminal nanoluciferase-tagged VEGFR2.

Sunitinib-red (Perkin Elmer) is a fluorescent derivative of sunitinib coupled to the Perkin Elmer d2 fluorescent dye (absorption 650nm, emission 670nm). Preliminary experiments were undertaken to assess the binding of sunitinib-red (100 nM) to intact HEK293T cells expressing a C-terminal nanoluciferase tagged VEGFR2 (VEGFR2-NLuc) using NanoBRET [32,33]. These experiments showed no significant increase in BRET over the vehicle control following a 1h incubation at 37 ^{o}C (Figure 1a). Several different dilutions of furimazine were evaluated as well as the impact of treatment with 1nM $VEGF_{165}$a (Figure 1a). The same cells were then lysed using NanoGlo® lytic buffer at room temperature for 10 minutes and BRET measured a second time. Under these conditions, there was a significant increase ($p<0.001$; paired t-test) in BRET ratio in those wells incubated with 100 nM sunitinib-red (Figure 1b). These data suggest that sunitinib-red is not cell permeable. A smaller signal ($p<0.001$; one-way ANOVA) was obtained in experiments when furimazine (1:400) was added at the beginning of the 1h incubation at 37 ^{o}C, and the presence of 1nM $VEGF_{165}$a had no significant effect on the ligand-binding signal obtained ($p>0.05$, One-way ANOVA; Figure 1b). The effect of increasing concentrations of sunitinib-red on ligand-binding was then assessed using a 1h incubation in the presence of 1nM $VEGF_{165}$a at 37 ^{o}C, followed by 10 min incubation with furimazine at 37 ^{o}C and then lysis of cells for 10 min at room temperature (Figure 2). Under these experimental conditions, sunitinib-red exhibited a clear saturable component of binding that could be inhibited by 100 μM cediranib (Figure 2a). The specific component of sunitinib-red binding yielded a log K_D value of -7.29 $\pm$ 0.06 (n=5 independent experiments; Figure 2b).

3.2 Effect of TKIs on sunitinib-red binding to VEGFR2-NLuc.

To assess the impact of TKIs on the binding of 30nM sunitinib-red, experiments were conducted as described above with a 1h incubation in the presence of 1nM $VEGF_{165}$a (for comparison with NFAT assays, see below) at 37 ^{o}C, followed by 10 min incubation with furimazine at 25 ^{o}C and then lysis of cells for 10 min at room temperature (Figure 3). The inhibitors chosen for study are given in Table 1 with their main tyrosine kinase targets also identified. Potent inhibition of sunitinib-red binding was obtained with sunitinib (Figure 3a), cediranib (Figure 3b) and motesanib (Figure 3c) (Table 2). Fostamatinib (Figure 3d) and its active metabolite R406 also showed moderate binding affinity (Figure 3e; Table 2). In the case of sunitinib, the inhibition curve was biphasic with an increase in BRET ratio occurring at concentrations above 1μM (Figure 3a). This is almost certainly due to the inherent fluorescence of non-labelled sunitinib [37]. The EGFR inhibitor erlotinib, the BCR-ABL inhibitor dasatinib and the second generation SYK inhibitors cerdulatinib and entospletinib were without significant effect at concentrations up to 1μM (Figure 3; Table 2).

3.3 Kinetic analysis of sunitinib-red binding.

To evaluate the impact of the different assay conditions on the kinetics of sunitinib-red binding, the time course of the change in BRET ratio was monitored every 60s (Figure 4). Figure 4a shows the time course of the standard conditions used above where cells were incubated for 1h in the presence of 1nM $VEGF_{165}$a and sunitinib-red at 37 ^{o}C, followed by 10 min incubation

with furimazine at 25 °C and then lysis of cells at 25 °C. In Figure 4a the time course is shown following the addition of furimazine. Ten minutes after addition of furimazine cells were lysed and the incubation continued for a further 50 min. The kinetic profile shows that at each of the three concentrations of sunitinib-red used there was a rapid increase in BRET ratio following cell lysis that reached a peak after 10 min and was then sustained for a further 40 min at 25 °C. Figure 4b shows the same experimental format apart from the fact that furimazine and lysis was undertaken at 37 °C and then maintained at this temperature for a further 50 min. It is clear from Figure 4b that a rapid peak in BRET ratio is obtained following lysis but this declines towards basal levels over the 50 min period. It is likely that this is due to furimazine depletion and is consistent with the lower values for sunitinib-stimulated BRET obtained when furimazine was added at the start of the experiment in Figure 1b.

In subsequent experiments, cells were lysed immediately following a 15 min incubation with 1nM $VEGF_{165}a$ and furimazine was added at the same time as the NanoGlo® lytic buffer. Sunitinib-red (with or without 100μM cediranib as required) was then added after 10min and the incubation continued for a further 50 min at 25 °C (Figure 4c) or 37 °C (Figure 4d). As before, the responses obtained at 37 °C (Figure 4d) were transient in nature and very similar to those obtained in Figure 4b). At 25 °C, the BRET signal obtained after addition of sunitinib-red was rapid and well maintained over the full time course measured (Figure 4c). Simultaneous fitting of the kinetic curves obtained for the three concentrations of sunitinib in Figure 4c allowed initial estimates of the k_{on} (2.04×10^7 $M^{-1}.min^{-1}$) and k_{off} (0.27 min^{-1}) rate constants of sunitinib-red to be made. This calculation was repeated for kinetic experiments conducted with five different of sunitinib-red (3,10,30,100,300nM; Figure 5a). Analysis of these data yielded kinetic constants for sunitinib-red of 3.96×10^7 $M^{-1}.min^{-1}$ (k_{on}) and 0.76 min^{-1} (k_{off}) consistent with a fast rate of association with the receptor and a short residence time (1.32 min; $1/k_{off}$). The kinetic log K_D value obtained from the k_{off} and k_{on} values was -7.72 and was similar to the value of -7.29 obtained in equilibrium binding experiments (Figure 2b). Plotting the specific binding obtained at 61 min in these kinetic experiments (Figure 5b) yielded a similar log K_D value of -7.56.

A notable feature of the time course obtained in the presence of both sunitinib-red and 100μM cediranib in lysed cells at 25 °C was that there was an overshoot of the BRET signal on first application of the ligands that then returned to much lower levels after a further 10 min incubation (Figure 4c, Figure 5a). This is most likely due to the rate of binding of cediranib being much slower than that of sunitinib-red and similar kinetic profiles have been seen for G protein-coupled receptor binding kinetics [38,39]. To investigate this further we undertook kinetic ligand-binding studies with different concentrations of the unlabelled TKIs cediranib, fostamatinib, dasatinib and entospletinib (Figure 6). In the case of the higher concentrations of both cediranib (Figure 6a) and fostamatinib (Figure 6c) there was an overshoot of sunitinib-red binding at the early time points that slowly declined to a new lower steady state level over 10-30 min as the antagonism by each unlabelled TKI developed. To evaluate the kinetic properties of both cediranib and fostamatinib we used the competition association analysis framework of Motulsky and Mahan (1984 [34]) to fit the baseline-corrected BRET ratios obtained following addition of TKIs (Figure 7). Simultaneous fitting of these data with shared values for k_{on} and k_{off} at each concentration of the unlabelled TKI yield the kinetic constants for cediranib (Figure 7a) and fostamatinib (Figure 7b) shown in Table 3. These data show that both inhibitors have long residence times (when compared to sunitinib-red) and slower k_{on} rates (Table 3). Kinetic studies were also undertaken with dasatinib (Figure 6b) and entospletinib (Figure 6d) in order to check that the lack of inhibition of binding was not due to an extremely slow equilibration with the receptor. However, the data clearly show that there

is no antagonism of sunitinib-red binding at any concentration of either of these two TKIs over the time course followed.

3.4 Effect of TKIs on $VEGF_{165}$a-stimulated NFAT luciferase reporter gene activity.

Carter *et al*. (2015;[30]) have previously described a nuclear factor of activated T-cells (NFAT)-luciferase assay to monitor the pharmacological interaction of TKIs on VEGFR2 signalling. Here, we have used this NFAT assay to compare the effect of TKIs on NanoBRET ligand-binding and signalling. Figure 8a shows the NFAT response to increasing concentrations of $VEGF_{165}$a over 5 h in HEK293 cells expressing the NFAT ReLuc2P vector and an N-terminal nanoluciferase-tagged VEGFR2 (NLuc-VEGFR2; [33]). The log EC_{50} value obtained for $VEGF_{165}$a obtained in five independent experiments was -9.85 ± 0.11 (n = 5). To determine whether the lack of binding of sunitinib-red in the NanoBRET assay was a consequence of poor penetration into the intracellular environment, we evaluated whether increasing concentrations of sunitinib-red could attenuate $VEGF_{165}$a-stimulated NFAT responses over 5h stimulation (Figure 8b). These data showed no significant inhibition of the response to 1nM $VEGFR_{165}$a at concentrations up to 300nM. At 1μM there was a marked and significant attenuation of the VEGF response (Figure 8b). These data are consistent with a poor penetration by sunitinib-red into the intracellular environment over the concentration range used (3nM – 300nM) for the NanoBRET ligand-binding experiments.

Potent inhibition of VEGF-stimulated NFAT responses was, however, obtained with unlabelled sunitinib (Figure 9a), cediranib (Figure 9b) and motesanib (Figure 9c) (Table 2). Fostamatinib (Figure 9d) and its active metabolite R406 produced a less potent inhibition of the VEGF response (Figure 9e; Table 2). The EGFR inhibitor erlotinib and the second generation SYK inhibitor cerdulatinib were without significant effect at concentrations up to 1μM (Figures 9f and 9g). However, in marked contrast to the data obtained in NanoBRET experiments with sunitinib-red, both dasatinib (log IC_{50} -6.96 ± 0.19, n=5; Figure 9h) and entospletinib (log IC_{50} -8.28 ± 0.21, n=5; Figure 9i) exhibited a marked attenuation of the response to VEGF (Table 2). To ascertain whether these two inhibitors were able to attenuate the NFAT signalling cascade independently of VEGF2-receptor activation we also evaluated them as inhibitors of the response to the calcium ionophore ionomycin (1μM; Figure 10). Both TKIs inhibited the ionomycin response with similar potencies as those found for the VEGF-response (Figure 10). The log IC_{50} values obtained of -7.16 ± 0.22 (n=5; dasatinib) and 8.18 ± 0.08 (n=5; entospletinib) were not significantly different ($p>0.05$; unpaired t-test) from those obtained with VEGF as agonist.

4. Discussion

In the present study we have used a fluorescent analogue of sunitinib (sunitinib-red) and NanoBRET to directly monitor the binding of TKIs to VEGFR2. This is based on a proximity-based assay that requires the fluorescent and bioluminescent components to be within 10nm of each other for BRET to occur (Figure 11a) [40]. This has been used to quantify the direct interactions between sunitinib-red and the C-terminus of VEGFR2 tagged with the bright bioluminescent protein nanoluciferase [31-33]. Sunitinib is an example of a type 1 TKI that recognises the active conformation of the kinase domain of VEGFR2 and competes with ATP for the ATP binding-site within the VEGFR2 kinase domain [41]. In this study we treated cells with 1nM $VEGF_{165}$a prior to monitoring the binding of sunitinib-red to put the receptor into the active conformation and to maintain consistency with the presence of 1nM $VEGF_{165}$a in the functional NFAT reporter gene assay [30,33] that was used for comparison. However, in the absence of 1nM VEGF there was no significant attenuation of the specific binding of sunitinib-red (Figure 1).

A key feature of the binding studies with sunitinib-red was that no specific binding was detected in intact cells. Binding was only detected when the cells were lysed. This suggests that sunitinib-red was membrane impermeable and not able to access the intracellular kinase domain of VEGFR2 unless the cells were lysed. This was confirmed in studies of the effect of sunitinib-red on the VEGF-stimulated NFAT reporter gene response in intact cells, where significant inhibition was only obtained after 5h incubation at the highest concentration of sunitinib-red used (1μM). Over the concentration range used in the majority of NanoBRET binding assays (3 – 300nM) there was no significant inhibition of the NFAT response. In subsequent experiments, cells were incubated with $VEGF_{165}$a, sunitinib-red and competing TKIs for 1h at 37^{o}C, before addition of the nanoluciferase substrate furimazine [40] and lysis for 10 min at 25 °C. Using this standard approach, sunitinib-red exhibited specific binding to the kinase domain of VEGFR2 with a log K_D of -7.29 that could be inhibited by a range of TKIs including sunitinib, cediranib and the SYK inhibitor fostamatinib (and its active metabolite R406), known to bind to VEGFR2 and lead to hypertension [15,16,18,21,42]. In marked contrast, the EGFR inhibitor erlotinib, the BCR-ABL inhibitor dasatinib and the second generation SYK inhibitors cerdulatinib and entospletinib were without significant effect, consistent with their reported low binding affinity for VEGFR2 [21,23,24].

Kinetic analysis of the time course of sunitinib-red binding following lysis of cells at 25 °C confirmed that 10 min was sufficient for sunitinib-red to reach equilibrium and the response was well maintained for a further 40 min. If lysis was undertaken at 37 °C, the peak response was achieved within 5 min, but was not sustained and declined towards basal levels over the next 45 min. This is likely to be due to depletion of the furimazine substrate. If cells were lysed before addition of sunitinib-red the NanoBRET signal following sunitinib-red addition showed a very similar time course to that achieved in the previous assay format (where sunitinib-red was incubated for 1h at 37 °C before lysis; Figure 4). However, a notable feature of the response obtained in lysed cells when 100nM sunitinib-red and 100μM cediranib were added simultaneously was that there was an overshoot of the BRET signal on first application of the ligands that then returned to much lower levels. This suggested that cediranib associated with the ATP-binding site of the kinase domain of VEGFR2 at a much slower rate than sunitinib-red. This is characteristic of competing ligands that have a very slow off rate and take much longer to reach equilibrium than the labelled compound [38,39]. We therefore used the Motulsky and Mahan (1984; [34]) method to fit competition association kinetic curves for different concentrations of cediranib and a fixed concentration (30nM) of sunitinib-red (Figure 6A, 7A). This analysis confirmed that cediranib had a much longer retention time ($1/k_{off}$; 112.4 min) than sunitinib-red (1.3 min) (Table 3). A similar analysis indicated that fostamatinib had a similar slow dissociation from the ATP-binding site of VEGFR2 (retention time of 140.9 min). This latter effect almost certainly reflects the kinetics of its active metabolite R406 since fostamatinib is rapidly hydrolysed by cellular alkaline phosphatases to R406 [43,44]. Consistent with this, fostamatinib and R406 were very similar in their ability to inhibit sunitinib-red binding and $VEGF_{165}$a-stimulated NFAT responses (Table 2).

We have previously used an NFAT-luciferase assay to monitor the pharmacological interaction of TKIs with VEGFR2 signalling [30,33]. This assay is based on the effect of VEGFR2 activation leading to phosphorylation and activation of phospholipase γ resulting in the release of intracellular calcium ions that then activate calcineurin. This leads to dephosphorylation of NFAT which allows NFAT to enter the nucleus and interact with the NFAT response element within the promoter of the luciferase gene (Figure 11b). We therefore compared the results from sunitinib-red binding with those obtained in parallel experiments investigating the potencies of TKIs as inhibitors of $VEGF_{165}$a-stimulated NFAT reporter gene responses. These data confirmed that those TKIs that inhibited the specific binding of sunitinib-red to VEGFR2 also inhibited $VEGF_{165}$a-mediated NFAT responses with a similar potency. As expected, the EGFR inhibitor erlotinib and SYK inhibitor cerdulatinib were without significant effect on the $VEGF_{165}$a induced NFAT response. However, a surprising feature of these data was the fact that the BCR-ABL inhibitor dasatinib [45-47] and the SYK inhibitor entospletinib [23] were able to attenuate VEGFR2 signalling without a direct inhibition of the specific binding of sunitinib-red to VEGFR2. Interestingly, dasatinib has also been reported to inhibit the phosphorylation of SYK [45,46]. It is possible that the attenuation of VEGFR2-signalling by dasatinib and entospletinib is a consequence of a SYK binding site being created on VEGFR2 following $VEGF_{165}$a-induced VEGFR2 dimerization which brings together two hemi-ITAM sequences of VEGFR2 [28]. These hemi-ITAM sequences begin at Y1175 on the intracellular C-terminal tail of VEGFR2 [28] and phosphorylation of Y1175 recruits PLCγ that triggers Ca^{2+}-dependent signalling and is involved in endothelial cell migration [5]. However, the lack of effect of the second generation of SYK inhibitor cerdulatinib [24,36] on $VEGF_{165}$a-stimulated NFAT responses would seem to rule this out.

To investigate whether other off-target kinases are involved in the inhibition produced by dasatinib and entospletinib, we also evaluated their ability to inhibit ionomycin-stimulated NFAT responses. The calcium ionophore ionomycin was used to generate directly an influx

of calcium ions into cells so that they can directly stimulate the phosphatase activity of calcineurin leading to the dephosphorylation and thus bypass the need for VEGFR2 to activate PLCγ (Figure 11b). Both TKIs inhibited ionomycin-stimulated NFAT responses with a similar potency to that determined for inhibition of $VEGF_{165}$a-mediated responses. NFAT proteins are normally hyper-phosphorylated and retained in the cytoplasm. Following calcium mobilization, NFAT is dephosphorylated by the calcium-calmodulin-activated protein phosphatase calcineurin which exposes a nuclear localization signal leading to its translocation to the nucleus [48]. NFAT then cooperates with other transcription factors to regulate transcription by binding to the NFAT response element (Figure 11b) [48]. The data obtained with dasatinib and entospletinib suggest that it is interference with some of these down-stream signalling proteins that is responsible for the attenuation of VEGFR2-mediated NFAT responses (Figure 11b).

In summary, we report here the development of a ligand-binding assay using sunitinib-red and NanoBRET to monitor the direct interactions of TKIs with the kinase domain of VEGFR2. Sunitinib-red is not membrane permeable but can be used to monitor the binding affinity and kinetics of a range of TKIs in cell lysates. Kinetic studies show that sunitinib-red binds rapidly to VEGFR2 at 25 °C and that cediranib has slower binding kinetics with an average residence time of 112 min. Comparison between the log K_i values for inhibition of binding of sunitinib-red and log IC_{50} values for attenuation of $VEGF_{165}$a-stimulated NFAT responses showed very similar values for compounds that inhibited sunitinib-red binding. However, two compounds that failed to inhibit sunitinib-red binding (dasatinib and entospletinib) were still able to attenuate VEGFR2-mediated NFAT signalling through inhibition of downstream signalling events. These results suggest that these compounds may still exhibit cardiovascular liabilities resulting from interference with VEGFR2 signalling. From this perspective it is interesting that pulmonary arterial hypertension is a reported adverse effect of dasatinib [49].

Author contributions

Conceived the study: Hill, Kilpatrick, Woolard.

Participated in research design: Van Daele, Kilpatrick, Woolard, Hill,

Conducted experiments: Van Daele

Performed data analysis: Van Daele, Hill

Wrote or contributed to the writing of the manuscript: Van Daele, Kilpatrick, Woolard, Hill.

Decalaration of interest

The authors declare that they have no known competing financial interests or personal relationships that could have appeared to influence the work reported in this paper.

Acknowledgements

This work was supported the H2020 Marie Skłodowska-Curie Actions (grant number GA858070) and MRC Grant MR/N020081/1. L.E.K was supported by a University of Nottingham Anne McLaren Fellowship. The graphical abstract and Figure 11 were prepared using biorender.com.

References.

[1] N. Ferrara. Vascular endothelial growth factor: basic science and clinical progress. Endocr Rev. 25 (2004) 581-611.

[2] N. Ferrara. VEGF-A: a critical regulator of blood vessel growth. Eur Cytokine Netw. 20 (2009)158-63.

[3] M. Shibuya. Vascular Endothelial Growth Factor (VEGF) and Its Receptor (VEGFR) Signaling in Angiogenesis: A Crucial Target for Anti- and Pro-Angiogenic Therapies. Genes Cancer. 2 (2011)1097-105.

[4] R.M.Touyz, N.N. Lang, J. Herrmann, A.H. van den Meiracker, A.H.J. Danser. Recent advances in hypertension and cardiovascular toxicities with vascular endothelial growth factor inhibition. Hypertension. 70 (2017) 220-226.

[5] C.J. Peach, V.W. Mignone, M.A. Arruda, D.C. Alcobia, S.J. Hill, L.E. Kilpatrick, J. Woolard. Molecular Pharmacology of VEGF-A Isoforms: Binding and Signalling at VEGFR2. Int J Mol Sci. 19 (2018) 1264.

[6] S. Koch, S.Tugues, X. Li, L. Gualandi, L. Claesson-Welsh. Signal transduction by vascular endothelial growth factor receptors. Biochem J. 437 (2011) 169-83.

[7] K. Holmes, O.L Roberts, A.M. Thomas, M.J. Cross. Vascular endothelial growth factor receptor-2: structure, function, intracellular signalling and therapeutic inhibition. Cell Signal.19 (2007) 2003-12.

[8] K.J. Gotink, H.M. Verheul. Anti-angiogenic tyrosine kinase inhibitors: what is their mechanism of action? Angiogenesis. 13 (2010) 1-14.

[9] P. Carmeliet. Angiogenesis in life, disease and medicine. *Nature 438* (2005) 932–36.

[10] N. Dey, P De, L.J. Brian. Evading anti-angiogenic therapy: resistance to anti-angiogenic therapy in solid tumors. Am J Transl Res. 7 (2015)1675-98.

[11] J. Folkman. What is the evidence that tumors are angiogenesis dependent? J Natl Cancer Inst. 82(1990) 4-6.

[12] N. Ferrara, A.P. Adamis. Ten years of anti-vascular endothelial growth factor therapy. Nat Rev Drug Discov. 15 (2016) 385-403.

[13] F. Musumeci, M. Radi, C. Brullo, S. Schenone. Vascular endothelial growth factor (VEGF) receptors: drugs and new inhibitors. J Med Chem. 55 (2012) 10797-822.

[14] S. Faivre, G. Demetri, W. Sargent, E. Raymond. Molecular basis for sunitinib efficacy and future clinical development. Nat Rev Drug Discov. 6 (2007) 734-45.

[15] J.J. Carter, L.V. Fretwell, J. Woolard. Effects of 4 multitargeted receptor tyrosine kinase inhibitors on regional hemodynamics in conscious, freely moving rats. FASEB J. 31 (2017) 1193-1203.

[16] S.L. Cooper, J.J. Carter, J. March, J. Woolard. Long-term cardiovascular effects of vandetanib and pazopanib in normotensive rats. Pharmacol Res Perspect. 7 (2019) e00477.

[17] H.X. Chen, J.N. Cleck. Adverse effects of anticancer agents that target the VEGF pathway. Nat Rev Clin Oncol. 6 (2009) 465-77.

[18] T. Collins, K. Gray, M. Bista, M. Skinner, C. Hardy, H. Wang, J.T. Mettetal, A.R. Harmer. Quantifying the relationship between inhibition of VEGF receptor 2, drug-induced blood pressure elevation and hypertension. Br J Pharmacol. 175 (2018) 618-630.

[19] N.T. Connell, N. Berliner. Fostamatinib for the treatment of chronic immune thrombocytopenia. Blood. 133 (2019) 2027-2030.

[20] A. Newland, V. McDonald. Fostamatinib: a review of its clinical efficacy and safety in the management of chronic adult immune thrombocytopenia. Immunotherapy. 12 (2020) 1325-1340.

[21] M.I. Davis, J.P.Hunt, S. Herrgard, P. Ciceri, L.M. Wodicka, G. Pallares, M. Hocker, D.K. Treiber, P.P Zarrinkar. Comprehensive analysis of kinase inhibitor selectivity. Nat Biotechnol. 29 (2011) 1046-51.

[22] M.E. Weinblatt, A. Kavanaugh, M.C. Genovese, T.K. Musser, E.B. Grossbard, D.B. Magilavy. An oral spleen tyrosine kinase (Syk) inhibitor for rheumatoid arthritis. N Engl J Med. 363 (2010) 1303-12.

[23] K.S. Currie, J.E. Kropf, T. Lee, P. Blomgren, J. Xu, Z. Zhao, S. Gallion, J.A. Whitney, D. Maclin, E.B. Lansdon, P. Maciejewski, A.M. Rossi, H. Rong, J. Macaluso, J. Barbosa, J.A. Di Paolo, S.A. Mitchell. Discovery of GS-9973, a selective and orally efficacious inhibitor of spleen tyrosine kinase. J Med Chem. 57 (2014) 3856-73.

[24] D. Liu, A. Mamorska-Dyga. Syk inhibitors in clinical development for hematological malignancies. J Hematol Oncol. 10 (2017) 145.

[25] A. Mócsai, J. Ruland, V.L.Tybulewicz. The SYK tyrosine kinase: a crucial player in diverse biological functions. Nat Rev Immunol.10 (2010) 387-402.

[26] C.E. Hughes, A.Y. Pollitt, J. Mori, J.A. Eble, M.G.Tomlinson, J.H. Hartwig, C.A. O'Callaghan, K. Fütterer, S.P. Watson. CLEC-2 activates Syk through dimerization. Blood. 115 (2010) 2947-55.

[27] B. Bauer, A. Steinle. HemITAM: A single tyrosine motif that packs a punch. Sci Signal. 10 (2017) eaan3676.

[28] S. Kazerounian, M. Duquette, M.A. Reyes, J.T. Lawler, K. Song, C. Perruzzi, L. Primo, R. Khosravi-Far, F. Bussolino, J. Rabinovitz, J. Lawler. Priming of the vascular endothelial growth factor signaling pathway by thrombospondin-1, CD36, and spleen tyrosine kinase. Blood. 117 (2011) 4658-66.

[29] N. de Jesus-Gonzalez, E. Robinson, J. Moslehi, B.D. Humphreys. Management of antiangiogenic therapy-induced hypertension. Hypertension. 60 (2012) 607-15.

[30] J.J. Carter, A.J. Wheal, S.J. Hill, J. Woolard. Effects of receptor tyrosine kinase inhibitors on VEGF165 a- and VEGF165 b-stimulated gene transcription in HEK-293 cells expressing human VEGFR2. Br J Pharmacol. 172 (2015) 3141-50.

[31] T. Machleidt, C.C. Woodroofe, M.K. Schwinn, J. Méndez, M.B. Robers, K. Zimmerman, P. Otto, D.L. Daniels, T.A. Kirkland, K.V. Wood. NanoBRET-A Novel BRET Platform for the Analysis of Protein-Protein Interactions. ACS Chem Biol. 10 (2015) 1797-804.

[32] L. Stoddart, E.K.M. Johnstone, A.J. Wheal, J. Goulding, M.B. Robers, T. Machleidt, K.V. Wood, S.J. Hill, K.D.G. Pfleger. Application of BRET to monitor ligand binding to GPCRs. *Nat. Methods 12* (2015) 661–63.

[33] L.E. Kilpatrick, R. Friedman-Ohana, D.C. Alcobia, K. Riching, C.J. Peach, A.J. Wheal, S.J. Briddon, M.B. Robers, K. Zimmerman, T. Machleidt, K.V. Wood, J. Woolard, S.J. Hill. Real-time analysis of the binding of fluorescent $VEGF_{165}$a to VEGFR2 in living cells: Effect of receptor tyrosine kinase inhibitors and fate of internalized agonist-receptor complexes. Biochem Pharmacol. 136 (2017) 62-75.

[34] H.J. Motulsky, L.C. Mahan. The kinetics of competitive radioligand binding predicted by the law of mass action. Mol Pharmacol. 25 (1984) 1-9.

[35] K.B. Neves, A.C. Montezano, N.N. Lang, R.M. Touyz. Vascular toxicity associated with anti-angiogenic drugs. Clin Sci (Lond). 134 (2020) 2503-2520.

[36] G Coffey, A. Betz, F. DeGuzman, Y. Pak, M. Inagaki, D.C. Baker, S.J. Hollenbach, A. Pandey, U. Sinha. The novel kinase inhibitor PRT062070 (Cerdulatinib) demonstrates efficacy in models of autoimmunity and B-cell cancer. J Pharmacol Exp Ther. 351 (2014) 538-48.

[37] P. Nowak-Sliwinska, A. Weiss, J.R. Van Beijnum, T.J. Wong, W.W. Kilarski, G. Szewczyk, H.M. Verheul, T. Sarna, H. van den Bergh, A.W. Griffioen. Photoactivation of lysosomally sequestered sunitinib after angiostatic treatment causes vascular occlusion and enhances tumor growth inhibition. Cell Death Dis. 6(2015) e1641.

[38] F. Schiele, P. Ayaz, A. Fernández-Montalván. A universal homogeneous assay for high-throughput determination of binding kinetics. Anal Biochem. 468 (2015) 42-9.

[39] M. Bouzo-Lorenzo, L.A. Stoddart, L. Xia, A.P. IJzerman, L.H. Heitman, S.J. Briddon, S.J. Hill. A live cell NanoBRET binding assay allows the study of ligand-binding kinetics to the adenosine A_3 receptor. Purinergic Signal.15 (2019) 139-153.

[40] M.P. Hall, J. Unch, B.F. Binkowski, M.P. Valley, B.L. Butler, M.G. Wood, P. Otto, K. Zimmerman, G. Vidugiris, T. Machleidt, M.B. Robers, H.A. Benink, C.T. Eggers, M.R. Slater, P.L. Meisenheimer, D.H. Klaubert, F. Fan, L.P. Encell, K.V. Wood. Engineered luciferase reporter from a deep sea shrimp utilizing a novel imidazopyrazinone substrate. *ACS Chem. Biol. 7* (2012) 1848–57.

[41] F. Shaik, G.A. Cuthbert, S. Homer-Vanniasinkam, S.P Muench, S. Ponnambalam, M.A. Harrison. Structural Basis for Vascular Endothelial Growth Factor Receptor Activation and Implications for Disease Therapy. Biomolecules.10 (2020) 1673.

[42] M. Skinner, K. Philp, D. Lengel, L. Coverley, E. Lamm Bergström, P. Glaves, H. Musgrove, H. Prior, M. Braddock, R. Huby, J.O. Curwen, P. Duffy, A.R. Harmer. The contribution of VEGF signalling to fostamatinib-induced blood pressure elevation. Br J Pharmacol. 171 (2014) 2308-20.

[43] D.J. Sweeny, W. Li, J. Clough, S. Bhamidipati, R. Singh, G. Park, M. Baluom, E. Grossbard, D.T. Lau. Metabolism of fostamatinib, the oral methylene phosphate prodrug of the spleen tyrosine kinase inhibitor R406 in humans: contribution of hepatic and gut bacterial processes to the overall biotransformation. Drug Metab Dispos. 38 (2010) 1166-76.

[44] R. Matsukane, K. Suetsugu, T. Hirota, I. Ieiri. Clinical Pharmacokinetics and Pharmacodynamics of Fostamatinib and Its Active Moiety R406. Clin Pharmacokinet. 61 (2022) 955-972.

[45] K. Futosi, T. Nemeth, R. Pick, T. Vantus, B. Walzog, A Mocsai. Dasatinib inhibits proinflammatory functions of mature human neutrophils. Blood. 119 (2012) 4981-4991.

[46] A. Zarbock. The shady side of dasatinib. Blood.119 (2012) 4817-8.

[47] R. Chen, B. Chen. The role of dasatinib in the management of chronic myeloid leukemia. Drug Des Devel Ther. 9 (2015) 773-9.

[48] W. Zhang, T. Takahara, T. Achiha, H. Shibata, M. Maki. Nanoluciferase Reporter Gene System Directed by Tandemly Repeated Pseudo-Palindromic NFAT-Response Elements Facilitates Analysis of Biological Endpoint Effects of Cellular Ca^{2+}Mobilization. Int J Mol Sci.19 (2018) 605.

[49] F. Cheng, Q. Xu, Q. Li, Z. Cui, W. Li, F. Zeng. Adverse reactions after treatment with dasatinib in chronic myeloid leukemia: Characteristics, potential mechanisms, and clinical management strategies. Front Oncol.13 (2023) 1113462.

Table 1. Summary of the tyrosine kinase inhibitors (TKIs) used in the present study and their main tyrosine kinase targets.

TKI	Main targets	References
Sunitinib	VEGFRs, PDGFRs, c-KIT	[21,35]
Cediranib	VEGFRs, PDGFRs	[21,35]
Motesanib	VEGFRs, PDGFRs	[21]
Dasatinib	BCR-ABL, PDGFRs	[21]
Erlotinib	EGFR	[21]
Fostamatinib	SYK (1st generation)	[21]
R406	Active metabolite of fostamatinib	[21]
Cerdulatinib	SYK (2nd generation), Janus Kinase	[24,36]
Entospletinib	SYK (2nd generation)	[23,24]

Table 2. Summary of the potencies of tyrosine kinase inhibitors (TKIs) for inhibition of sunitinib-red binding to VEGFR2-NLuc and $VEGF_{165}$a-stimulated NFAT reporter gene responses. Values show the log dissociation constants (log K_i) determined from inhibition of sunitinib-red binding or log IC_{50} values for inhibition of NFAT responses to 1nM $VEGF_{165}$a. Mean K_i (nM) and IC_{50} (nM) are also shown. Data are mean ± SEM of 5 independent experiments, each performed in triplicate. NI, no inhibition.

TKI	Inhibition of sunitinib-red binding (log K_i)	Inhibition of sunitinib-red binding K_i (nM)	Inhibition of NFAT response to $VEGF_{165}$a (log IC_{50})	Inhibition of NFAT response to $VEGF_{165}$a IC_{50} (nM)
Sunitinib	-8.20 ± 0.13	6.3	-7.90 ± 0.12	12.6
Cediranib	-8.24 ± 0.12	5.8	-8.73 ± 0.02	1.9
Motesanib	-8.01 ± 0.10	9.8	-7.97 ± 0.10	10.7
Fostamatinib	-6.71 ± 0.12	195.0	-6.58 ± 0.32	263.0
R406	-6.44 ± 0.11	363.1	-6.87 ± 0.06	134.9
Erlotinib	NI		NI	
Cerdulatinib	NI		NI	
Dasatinib	NI		-6.96 ± 0.19	109.6
Entospletinib	NI		-8.28 ± 0.21	5.2

Table 3. Summary of kinetic parameters for tyrosine kinase inhibitors (TKIs) determined from analysis of association kinetic experiments**.** Rate constants for sunitinib-red were determined from the data presented in Figure 5. Rate constants for cediranib and fostamatinib were determined from the data presented in Figures 6 and 7 using the competitive association kinetics analysis of Motulsky & Mahan (1984; 34]). Retention time is given as the reciprocal of the k_{off} rate constant.

TKI	k_{on} ($M^{-1}.min^{-1}$)	k_{off} (min^{-1})	Retention time (min)	Kinetic log K_D
Sunitinib-red	3.96×10^7	0.76	1.32	-7.72
Cediranib	4.44×10^6	0.0089	112.36	-8.70
Fostamatinib	3.17×10^5	0.0071	140.86	-7.65

Figure legends.

Figure 1. Binding of 100nM sunitinib-red to HEK293T cells expressing VEGFR2-NLuc. (a) Cells were pre-incubated in the presence or absence (grey columns) of 1 nM $VEGF_{165}$a for 15 min, followed by 100nM sunitinib-red for a further 1 h at 37 °C/5% CO_2. Furimazine (1:400) was added to each well and the plates were incubated for a further 10 minutes at 37 °C/5% CO_2 before BRET ratios were then determined. In some wells, furimazine was added at higher concentrations (1:200, 1:100; orange and yellow columns). (b) The cells in (a) were lysed using NanoGlo® lytic buffer at room temperature for 10 minutes and BRET measured a second time. Values represent mean ± S.E.M from 5 individual experiments. Within each individual experiment triplicate determinations were made. * $p<0.001$ compared to corresponding vehicle control (paired t test). ** $p<0.001$ compared to sunitinib-red obtained following lysis in the presence of 1:400 furimazine (one-way ANOVA with posthoc Tukey's multiple comparison test). There was no significant difference between the data obtained (furimazine 1:400) in the presence or absence of 1nM $VEGF_{165}$a ($p>0.05$; one-way ANOVA with posthoc Tukey's multiple comparison test).

Figure 2. NanoBRET saturation binding studies with sunitinib-red. HEK293T cells expressing VEGFR2-NLuc were treated with increasing concentrations of sunitinib-red in the presence or absence of 100μM cediranib to define non-specific binding. (a) total and non-specific binding and (b) specific binding of sunitinib-red. Values represent mean ± S.E.M from 5 individual experiments. Within each individual experiment triplicate determinations were made.

Figure 3. Inhibition of the specific-binding of 30nM sunitinib-red by various TKIs. Non-specific binding was determined in the presence of 100μM cediranib. BRET ratios are expressed as a percentage of the specific binding of 30nM sunitinib-red. Values represent mean ± S.E.M from 5 individual experiments. Within each individual experiment triplicate determinations were made. (a) Sunitinib; (b) Cediranib; (c) Motesanib; (d) Fostamatinib; (e) R406; (f) Erlotinib; (g) Cerdulatinib; (h) Dasatinib; (i) Entospletinib.

Figure 4. Time course of the change in BRET ratio induced by different concentrations of sunitinib-red (sun-red) following lysis of cells under different experimental conditions. (a) The standard conditions used where cells were incubated in the presence of 1nM $VEGF_{165}$a for 15 min followed by sunitinib-red for a further 1h at 37°C. Where appropriate cediranib (ced; 100μM) was added simultaneously with sunitinib-red. This was then followed by 10 min incubation with furimazine at 25°C before lysis of cells at 25 °C. BRET ratios were measured every 60s for a further 50 min. (b) The same conditions as in (a) except that incubation with furimazine and lysis was conducted at 37°C and the incubations continued for a further 50min at 37°C. (c,d) Following a 15 min incubation with 1nM $VEGF_{165}$a, cells were lysed immediately. Furimazine was added at the same time as the NanoGlo® lytic buffer and incubated at 25 °C (c) or 37 °C (d). After 10 min, sunitinib-red (with or without 100μM cediranib as required) was added and the incubation continued for a further 50 min at 25°C (c) or 37°C (d). Values represent mean ± S.E.M from 5 individual experiments. Within each individual experiment triplicate determinations were made.

Figure 5. Time course of the change in BRET ratio induced by five different concentrations of sunitinib-red (sun-red). (a) Experiments were conducted under the same conditions as used in Figure 4(c) and BRET ratios were monitored every 60s. (b) Specific binding obtained at 61 min at different concentrations of sunitinib-red following subtraction of non-specific binding (determined in the presence of 100μM cediranib). In both (a) and (b) values represent mean ± S.E.M from 5 individual experiments. Within each individual experiment triplicate determinations were made.

Figure 6. Time course of the inhibition of 30nM sunitinib-red binding by different concentrations of TKIs. Experiments were conducted under the same conditions as used in Figure 4(c) at 25 ^{o}C and BRET ratios were monitored every 60s. Sunitinib-red (sun-red; 30nM) and unlabelled TKIs were added simultaneously at 10 min. (a) Cediranib (ced); (b) Dasatinib (dasa); (c) Fostamatinib (fosta); (d) Entospletinib (ento). Values represent mean ± S.E.M from 5 individual experiments. Within each individual experiment triplicate determinations were made at each time point.

Figure 7. Baseline corrected BRET ratios for inhibition of 30nM sunitinib-red (sun-red) binding by increasing concentrations of (a) cediranib (ced) or (b) fostamatinib (fosta). Data are taken from Figures 6(a) and 6(c) respectively. For baseline correction, the BRET ratio obtained immediately prior to sunitinib-red addition was subtracted from the BRET ratios obtained at all subsequent time points. Time on the x axis represents the time since ligand addition. Addition of sunitinib-red (sun-red; 30nM) and unlabelled TKIs therefore represents time zero. For each TKI, data points at each concentration were then fitted simultaneously with common values for k_{on}, k_{off} and maximum specific binding using the competitive ligand association method of Motulsky and Mahan (1984; [34]) within GraphPad Prism. The lines through each set of data represent the best-fit from this analysis. The k_{on} (3.96×10^{7} M^{-1} min^{-1}) and k_{off} (0.76 min^{-1}) rate constants for sunitinib-red binding (in the absence of inhibitor) used in this analysis were determined from the data presented in Figure 5. The k_{on} and k_{off} values obtained for cediranib and fostamatinib from this analysis are shown in Table 3.

Figure 8. NFAT-mediated gene transcription in response to $VEGF_{165}$a. (a) HEK293 cells stably expressing the NFAT ReLuc2P vector and NLuc-VEGFR2 were stimulated for 5h with $VEGF_{165}$a at 37^{o}C. Values are normalised to the response to 10nM $VEGF_{165}$a. (b) The effect of different concentrations of sunitinib-red on the NFAT response to 1nM $VEGF_{165}$a. Cells were pre-treated for 1h with sunitinib-red before 1nM $VEGF_{165}$a was added for a further 5 h. * $p<0.001$ with respect to the response to 1nM $VEGF_{165}$a in the absence of sunitinib-red (one-way ANOVA with posthoc Tukey's multiple comparison test). Values represent mean ± S.E.M from 5 individual experiments. Within each individual experiment triplicate determinations were made.

Figure 9. The effect of a range of TKIs on the NFAT response to 1nM $VEGF_{165}$a. NFAT-ReLuc2P HEK293 cells expressing the wild-type VEGFR2 were treated with increasing concentrations of inhibitor for 1h, followed by 1 nM $VEGF_{165}$a for a further 5h. Data are normalized to the maximal response to 1 nM $VEGF_{165}$a in the absence of inhibitor. Data are presented as mean ± SEM from 5 independent experiments, each performed in triplicate. (a) Sunitinib; (b) Cediranib; (c) Motesanib; (d) Fostamatinib; (e) R406; (f) Erlotinib; (g) Cerdulatinib; (h) Dasatinib; (i) Entospletinib.

Figure 10. The effect of (a) dasatinib and (b) entospletinib on the NFAT response to 1μM ionomycin. NFAT-ReLuc2P HEK293 cells expressing the wild-type VEGFR2 were treated with increasing concentrations of either (a) dasatinib or (b) entospletinib for 1h, followed by 1μM ionomycin for a further 5h. Data are normalized to the maximal response to 1μM ionomycin in the absence of inhibitor. Values represent mean ± S.E.M from 5 individual experiments. Within each individual experiment triplicate determinations were made.

Figure 11. Schematic showing (a) the binding of sunitinib-red to VEGFR2 and its inhibition by TKIs and (b) the basis of the VEGFR2-stimulated effect of VEGFR2 activation on calcium ion mobilization and subsequent dephosphorylation of hyper-phosphorylated NFAT by the phosphatase calcineurin. Sunitinib, cediranib, motesanib and R406 bind to the kinase domain of VEGFR2 to prevent binding of sunitinib-red and kinase activation. Dasatinib and entospletinib interrupt VEGFR2-mediated NFAT responses downstream of the effect of calcium ions on calcineurin.

Credit Author Statement.

BP-D-23-00877R1

Marieke Van Daele: methodology, investigation, writing – review & editing, formal analysis

Laura E Kilpatrick: conceptualization, methodology, writing – review & editing, supervision

Jeanette Woolard: conceptualization, writing – review & editing, supervision, funding acquisition.

Stephen J Hill: conceptualization, writing – original draft preparation, writing – review & editing, supervision, funding acquisition, project administration, formal analysis.